JOURNAL OF GEOPHYSICAL RESEARCH, VOL. 104, NO. C6, PAGES 13,381–13,394, JUNE 15, 1999

Mesoscale variations of biogeochemical properties in the Sargasso Sea

D. J. McGillicuddy Jr.,[1] R. Johnson,[2] D. A. Siegel,[3,4] A. F. Michaels,[5]
N. R. Bates,[2] and A. H. Knap[2]

Abstract. A mesoscale resolution biogeochemical survey was carried out in the vicinity of the U.S. Joint Global Ocean Flux Study Bermuda Atlantic Time-series Study (BATS) site during the summer of 1996. Real-time nowcasting and forecasting of the flow field facilitated adaptive sampling of several eddy features in the area. Variations in upper ocean nutrient and pigment distributions were largely controlled by vertical isopycnal displacements associated with the mesoscale field. Shoaling density surfaces tended to introduce cold, nutrient-rich water into the euphotic zone, while deepening isopycnals displaced nutrient-depleted water downward. Chlorophyll concentration was generally enhanced in the former case and reduced in the latter. Eddy-induced upwelling at the base of the euphotic zone was affected by features of two different types captured in this survey: (1) a typical mid-ocean cyclone in which doming of the main thermocline raised the near-surface stratification upward and (2) a mode water eddy composed of a thick lens of 18°C water, which pushed up the seasonal thermocline and depressed the main thermocline. Model hindcasts using all available data provide a four-dimensional context in which to interpret temporal trends at the BATS site and two other locations during the 2 weeks subsequent to the survey. Observed changes in near-surface structure at the BATS site included shoaling isopycnals, increased nutrient availability at the base of the euphotic zone, and enhanced chlorophyll concentration within the euphotic zone. These trends are explicable in terms of a newly formed cyclone that impinged upon the site during this time period. These observations reveal that eddy upwelling has a demonstrable impact on the way in which the nitrate-density relationship changes with depth from the aphotic zone into the euphotic zone. A similar transition is present in the BATS record, suggesting that eddy-driven upwelling events are present in the time series of upper ocean biogeochemical properties. The variability in main thermocline temperature and nitrate in this synoptic spatial survey spans the range observed in these quantities in the 10-year time series available at BATS to date (1988–1998).

1. Introduction

Interpretation of time series observations at fixed locations in the ocean is often complicated by the presence of spatial heterogeneity, which changes over time. The phenomenology to which this statement applies spans a tremendous range of space and timescales, from microscale patchiness to decadal fluctuations in the general circulation. Ultimately, the utility of time series measurements in terms of understanding oceanic processes is predicated on an ability to differentiate between spatial and temporal variability.

Several long-term, high-quality biogeochemical time series data have emerged at different points in the world ocean, including those offshore of Bermuda, Hawaii, California, and also station P in the subarctic Pacific. Typical sampling intervals of 1 month resolve the seasonal cycle, and interannual trends are clearly evident [e.g., *Michaels and Knap*, 1996]. However, superimposed on these signals are higher-frequency variations with amplitudes sometimes comparable to the explicitly resolved timescales. For example, *Doney* [1996] demonstrated that a significant fraction of the month-to-month variability observed in the Bermuda time series is associated with mesoscale three-dimensional processes. In attempting to deduce mechanistic understanding from such records, it is relevant to inquire about the nature of the unresolved phenomena and their net impact on the overall characteristics of the system.

Since its inception in 1988, the Bermuda Atlantic Time-series Study (BATS) has included periodic "validation" cruises to help better define the oceanographic context for the fixed-point time series measurements [*Michaels*, 1995; *Michaels and Knap*, 1996]. Early validation activities were aimed at determination of island effects on the offshore sampling location. In subsequent work, north-south transects were occupied to examine the large-scale meridional gradients in which the site is embedded [*Bates et al*., 1996]. More recently, validation efforts have been focused on the role of mesoscale phenomena. The

[1]Department of Applied Ocean Physics and Engineering, Woods Hole Oceanographic Institution, Woods Hole, Massachusetts.
[2]Bermuda Biological Station for Research, Ferry Reach, Bermuda.
[3]Institute for Computational Earth System Science, University of California, Santa Barbara.
[4]Also at Donald Bren School of Environmental Science and Management and Department of Geography, University of California, Santa Barbara.
[5]Wrigley Institute for Environmental Studies, University of Southern California, Avalon.

Paper number 1999JC900021.
0148-0227/99/1999JC900021$09.00

rationale for doing so is twofold: (1) to quantify the extent to which temporal changes at the time series site could be aliased spatial variability and (2) to better understand the impact of mesoscale fluctuations on biogeochemical processes themselves.

It has been recognized for some time that mesoscale processes could be involved in nutrient supply to the upper ocean. Comparison of two hydrographic profiles sampled 1 month apart in the summer of 1986 off Bermuda documented an apparently eddy-driven nutrient injection event that could account for 20–30% of the annual new production [*Jenkins*, 1988]. In the decade that has passed since those observations were first published, substantial evidence has accumulated that mesoscale eddies are the dominant mode of nutrient transport in the Sargasso Sea [*McGillicuddy et al*., 1998]. High-resolution regional numerical simulations in this area suggest eddy-induced upwelling causes intermittent fluxes of nitrate into the euphotic zone of magnitude sufficient to balance the nutrient demand implied by geochemical estimates of new production [*McGillicuddy and Robinson*, 1997]. Nitrate flux calculations based on satellite altimetry and a statistical model linking sea level anomaly to subsurface isopycnal displacements provide estimates of comparable order [*Siegel et al*., this issue]. Observations of a nutrient pulse associated with a mesoscale eddy were obtained using novel chemical sensing technology deployed on the Bermuda testbed mooring [*McNeil et al.*, 1999].

The eddy upwelling mechanism can be conceptualized by considering a density surface with mean depth coincident with the base of the euphotic zone. This surface is perturbed vertically by the formation, evolution, and destruction of mesoscale features. Shoaling density surfaces lift nutrients into the euphotic zone, which are rapidly utilized by the biota. Deepening density surfaces serve to push nutrient-depleted water out of the well-illuminated surface layers. The asymmetric light field thus rectifies vertical displacements of both directions into a net upward transport of nutrients, which is presumably balanced by a commensurate flux of sinking particulate material.

Direct observation of this process with traditional shipboard time series operations is made difficult by the spatial and temporal intermittency of the events. This issue is compounded by the mismatch in physical and biological timescales. With specific growth rates of the order of 1 per day [*Eppley*, 1972], phytoplankton populations are capable of nutrient utilization which is extremely rapid compared to the timescale of the supply mechanism (order weeks). Both of these characteristics drastically reduce the probability of detecting eddy-driven nutrient enhancements with biweekly to monthly observations at a single point. Time series of sufficient duration will eventually capture the statistical impact of temporally undersampled processes; however, a detailed understanding of the dynamics and distribution of these events is required for quantitative assessment of the sampling problem.

A coupled observational and modeling strategy was therefore adopted to achieve the two objectives of the BATS validation activities described above. The approach consisted of an initial spatial survey conducted in the vicinity of the time series site. Real-time analysis and data assimilation with a numerical model fed into an adaptive sampling strategy used to maximize the coverage of mesoscale features in the area. Numerical hindcasts were then used as a basis to interpret subsequent observations at the time series site in terms of the mesoscale evolution of the physical environment. Four-dimensional coupled biogeochemical simulations based on these data will be the subject of future work.

2. Methods

2.1. Hydrography and Biogeochemistry

A spatial biogeochemical survey was conducted June 26–30, 1996. The R/V *Weatherbird* occupied an adaptive grid of conductivity-temperature-depth (CTD) stations (to 700 m depth) with a horizontal resolution of 40 km, with expendable bathythermograph (XBT) drops (to 750 m depth) located in between, bringing the nominal station spacing down to 20 km (Figure 1). This spacing was chosen to be safely under the Rossby radius of deformation (45 km) in order to accurately resolve mesoscale phenomena. The 4-day survey was completed well within the decorrelation timescale of 30 days in this region [*Richman et al*., 1977] and therefore can be considered synoptic. Three biogeochemical stations along the southwestern boundary of the grid were reoccupied during the 2-week period following the survey. Cruise 96.1 of the Bermuda Bio-optics Program (BBOP) visited the BATS site (station 12) during July 4–6. Stations 11, 12, and 13 were reoccupied the following week (July 9–12) during BATS cruise 94. In addition, physical data (XBT and CTD) were gathered along portions of the northwest and southwest boundaries of the sampling domain during transits to and from Bermuda.

Discrete water samples were collected at each CTD station for assays of the following properties: nitrate, nitrite, phosphate, silicate, and chlorophyll. These measurements were made in accordance with the established BATS protocols [*Knap et al*., 1993]. Nutrient samples were analyzed at the surface and depths of 80, 100, 120, 140, 200, 300, 500, and 700 m. Chlorophyll was measured (using fluorometry) from the surface down to 140 m every 20 m.

2.2. Numerical Modeling of the Flow Field

Hydrographic observations were assimilated into a dynamical model to provide real-time nowcasts and forecasts to guide sampling strategy and to construct an optimal hindcast for subsequent interpretation of the biogeochemical data. The Harvard quasi-geostrophic (QG) open ocean model [see *Robinson and Walstad*, 1987, and references therein] was used for these purposes. Quantitative forecast skill has been demonstrated using this model in the Sargasso Sea [*Robinson and Leslie*, 1985; *Carton*, 1987; *Walstad and Robinson*, 1990], in addition to many other regions of the world ocean.

In this particular application, the open boundary model was configured with six vertical levels and 15-km horizontal resolution. Prognostic integrations require initial and boundary conditions for the model state variables (stream function and vorticity). These quantities were calculated from the density field derived from CTD and XBT measurements by the following procedure. First, dynamic height (referenced to 700 m) was computed from the density profiles (salinities corresponding to temperatures measured by XBT are taken from the mean temperature-salinity relationship for the region). These upper main thermocline observations were then extended throughout the water column via projection onto the baroclinic modes calculated from the mean Brunt-Väisälä frequency profile. This technique is particularly effective in the Sargasso Sea,

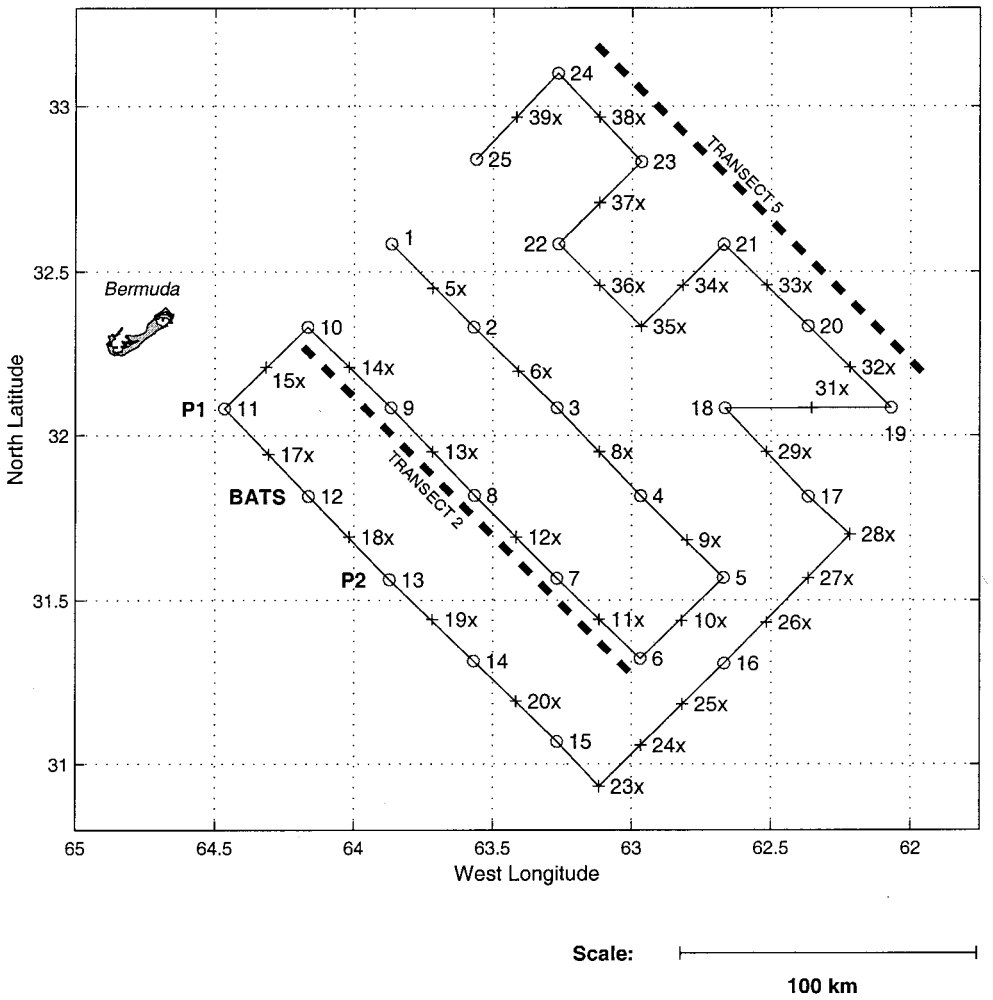

Figure 1. Survey pattern occupied on cruise BVAL16 of the Bermuda Atlantic Time-series Study (BATS) Validation, June 24–28, 1996. Conductivity-temperature-depth (CTD) stations are represented by circles, and expendable bathythermograph (XBT) stations are denoted by crosses. Thick dashed lines indicate the two transects from which the vertical sections are presented in Figure 2.

where it has been shown that approximately 65% of the available potential energy is contained in the first baroclinic mode and that the first three modes can account for approximately 90% of the same [*Richman et al.*, 1977]. The data are then mapped onto the model grid via objective analysis (OA) [*Carter and Robinson*, 1987] using a space-time correlation function derived from the nearby POLYMODE data set, which accounts for westward feature propagation [*Carton and McGillicuddy*, 1985]. This procedure thus provides a means to derive a nowcast for model initialization, as well as a statistical forecast (i.e., a time-dependent OA) of the boundary conditions necessary for dynamical model forecasts. In a hindcast mode, the same procedure was used to produce initial and boundary conditions from the ensemble of all available hydrographic observations.

3. Results

3.1. Feature Identification: Nowcasts, Forecasts, and Hindcasts

Assimilation of the survey data into a numerical model served two functions in this study: (1) to provide real-time nowcasts and forecasts of the flow field in order to guide at-sea sampling strategy and (2) to construct optimal field estimates using all available data in a hindcast mode for a posteriori interpretation not only of the biogeochemical survey but also of changes measured over time at selected locations (including the BATS site). The final hindcast created with all available observations (including additional transects along the northwestern and southwestern boundaries of the model domain in subsequent cruises) is displayed in Plate 1. The initial survey centered on June 28 reveals portions of four main features: two cyclonic and two anticyclonic. Cyclone C1 is located along the northwestern boundary of the domain, while the much weaker cyclone C2 lies to its south. A strong anticyclone AC1 occupies the eastern portion of the domain, flanked to its southwest by anticyclone AC2. According to the hindcast simulation for the following 2 weeks, cyclones C1 and C2 merge such that the center of the new feature resides well inside the model domain by July 12. Both AC1 and AC2 persist during this time period, although the eddy merger tends to intensify the jet located between the new cyclone and the adjacent anticyclones.

Although none of the features was sampled entirely, we interpret them as eddy structures as opposed to other forms of

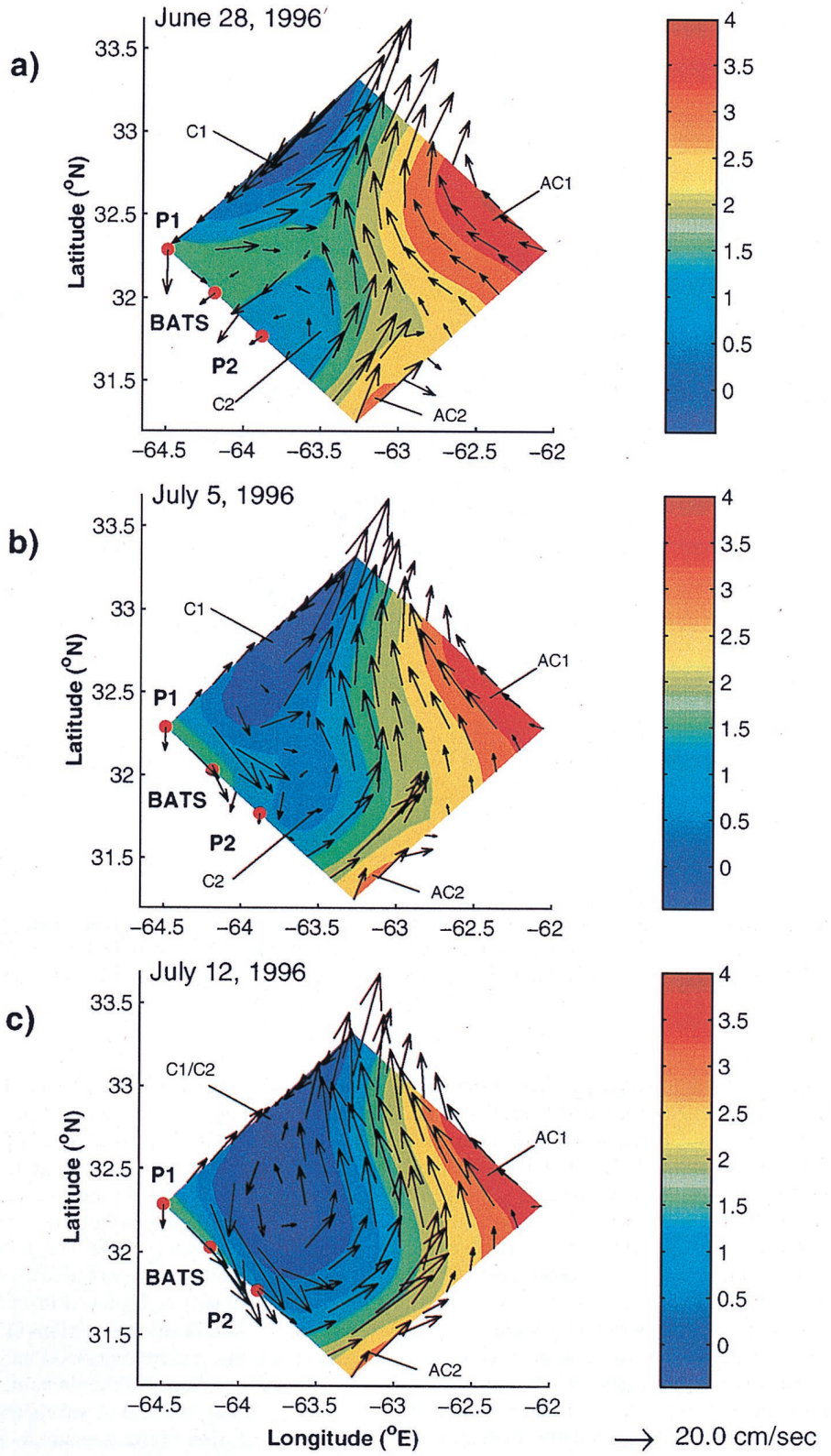

Plate 1. Final hindcast simulation for the period June 28 to July 12 1996: (a) initialization from the BVAL16 survey; (b) 7-day forecast, corresponding to the time of Bermuda Bio-optics Program (BBOP) cruise 96.1; and (c) 14-day forecast, corresponding to the time of BATS cruise 94. Color shading represents the nondimensional stream function field at 100 m; geostrophic velocity vectors are overlayed. Features C1, C2, AC1, and AC2 are identified (see text). Points P1, P2, and BATS indicate where biogeochemical measurements were made in the 2 weeks following the survey.

mesoscale variability such as meandering fronts. The dominance of eddy-driven mesoscale variability in this region has been well documented [*Richman et al*., 1977; *The MODE Group*, 1978; *Harrison and Heinmiller*, 1983; *Siegel et al*., this issue]. In fact, retrospective analysis of satellite altimetry for this time period (acquired subsequent to the seagoing operations) reveals sea level anomaly patterns that are consistent with the interpretation of the features observed here as eddies.

It is important to point out that the hindcast presented in Plate 1 is based upon an imperfect model using initial and boundary conditions that are not perfectly sampled. In order to assess the robustness of the model solutions, a sensitivity analysis was performed in which the model parameters, OA parameters, and treatment of the boundary conditions (i.e., persisted or time dependent) were systematically varied. Over a range of parameter choices spanning realistic limits, the qualitative characteristics of the model solutions remained the same, although quantitative differences were present. The hindcast was relatively insensitive to the treatment of boundary conditions, perhaps because the objectively analyzed boundary conditions changed little during this time period (Plate 1).

3.2. At-sea Forecasts and Sampling Strategy

The sampling strategy that led to the grid of stations shown in Figure 1 was guided by real-time nowcasts and forecasts of the mesoscale field produced via continuous assimilation of data during the cruise. The original plans were to orient a regular grid with respect to the topography so that the BATS site would be at the midpoint in the northeast-southwest direction. The survey began with the occupation of northwest-southeast transects, which commenced to the northeast of the BATS site and worked their way southwest. The very first transect cut across cyclone C1, revealing a strong mesoscale signal. As sampling progressed to the southwest, it became clear from the nowcasts that the southwestern extent of C1 had been defined. These transects identified two additional features (C2 and AC2), but they were much weaker than C1. The decision was therefore made to extend the grid to the northeast in order to gather more extensive observations in and around C1. In addition to achieving that objective, the effort resulted in the identification of the strong anticyclone AC1.

3.3. Vertical Structure

Along-track sections derived from the hydrographic observations demonstrate the impact of the eddies on the vertical structure of physical and biogeochemical properties (Figure 2). Transects 2 and 5 (identified in Figure 1) reveal the perturbations to the main thermocline associated with mesoscale features shown in Plate 1. Isotherm slopes surpass those in the climatological temperature field by an order of magnitude. Temperature contours shoal in the interior of cyclone C1, captured by the northwestern segments of both transects (Figure 2a). A detailed view of upper ocean thermal structure (Figure 2b) reveals a clear near-surface signature of this feature as a cold anomaly. Similar correspondence between the main thermocline signal and its surface manifestation is evident in anticyclone AC2 in the southeastern portion of transect 2: both the seasonal and main thermoclines are depressed in this typical warm eddy. The vertical structure of anticyclone AC1 is more complex. A thick lens of 18°C water tends to depress the main thermocline, while raising the seasonal thermocline. The former overshadows the latter by far in terms of its contribution to the geostrophic shear, resulting in the overall anticyclonic circulation in this feature. However, the most relevant aspect from a biogeochemical point of view is the lifting of the seasonal thermocline, which results in a cold temperature anomaly in the near-surface region.

To a large extent, the upper ocean nutrient distributions reflect the perturbations to the seasonal thermocline caused by the underlying eddy features (Figures 2c–2e). Nitrate, phosphate, and silicate concentrations are all enhanced within the boundaries of cyclone C1 and anticyclone AC1 and depressed in the interior of anticyclone AC2. These variations in nutrient availability are substantial: the 0.5 mmol m^{-3} nitrate isopleth actually outcrops at the 80-m depth horizon (well inside the euphotic zone) inside cyclone C1 and anticyclone AC1, while anticyclone AC2 causes nitrate concentration to be below the limit of detection all the way down to 140 m. Note that the outcropping of C1 is close to the edge of the feature (station 9) rather than its center. The mesoscale signal of nutrient enhancement associated with C1 is clearly evident in stations 8 and 9 of transect 2 and stations 23 and 24 of transect 5. Why this particular outcropping occurs at the edge of the feature is not known; submesoscale variability may play a role.

The most salient characteristic of the vertical distribution of chlorophyll is the pronounced subsurface maximum that occurs near the base of the euphotic zone (Figure 2f). Both the magnitude and vertical position of the deep chlorophyll maximum (DCM) are significantly altered by the presence of the eddies. Generally speaking, doming of the seasonal thermocline in cyclone C1 and anticyclone AC1 tends to shoal the DCM and increase the pigment concentration therein. Conversely, depression of the seasonal thermocline in anticyclone AC2 deepens the DCM and reduces its magnitude.

3.4. Horizontal Structure

To a large extent, horizontal variations observed in upper ocean physical properties reflect the underlying mesoscale structures (Plate 2). However, correspondence of near-surface distributions with the geostrophic pressure fields (Plate 1) is not exact owing to the intermingling of upper ocean processes with the main thermocline eddy motions. Temperature anomalies at 120 m associated with features C1 (cold), AC1 (cold), and AC2 (warm) are clearly evident (Plate 2a). Vertical coherence is most pronounced in the strongest eddy features, with cold anomalies collocated with C1 and AC1. The near-surface expression of AC2 is quite different; the warm anomaly extends approximately 50 km farther northwest than the depression in the main thermocline, such that the upper ocean manifestation of C2 is obscured.

Generally speaking, nutrient and pigment distributions are closely related to the hydrographic structure of the upper ocean. Density surfaces are domed upward in the interiors of cyclone C1 and anticyclone AC1, causing enhanced nitrate and phosphate concentrations therein (Plates 2b and 2c). Conversely, nutrient-depleted isopycnals are deepened inside AC2, resulting in nitrate and phosphate concentrations that are below the limit of detection throughout most of that feature at the 120-m depth horizon. Spatial variations in silicate concentration (Plate 2d) are of the order of the precision of the measurement (0.16 mmol m^{-3} [*Knap et al*., 1993]) and bear little resemblance to the patterns observed in other properties. This lack of mesoscale structure in the silicate data arises from a weak vertical gradient at the base of the euphotic zone and relatively large standard error in the chemical assay as compared with other quantities. Mean chlorophyll in the euphotic zone

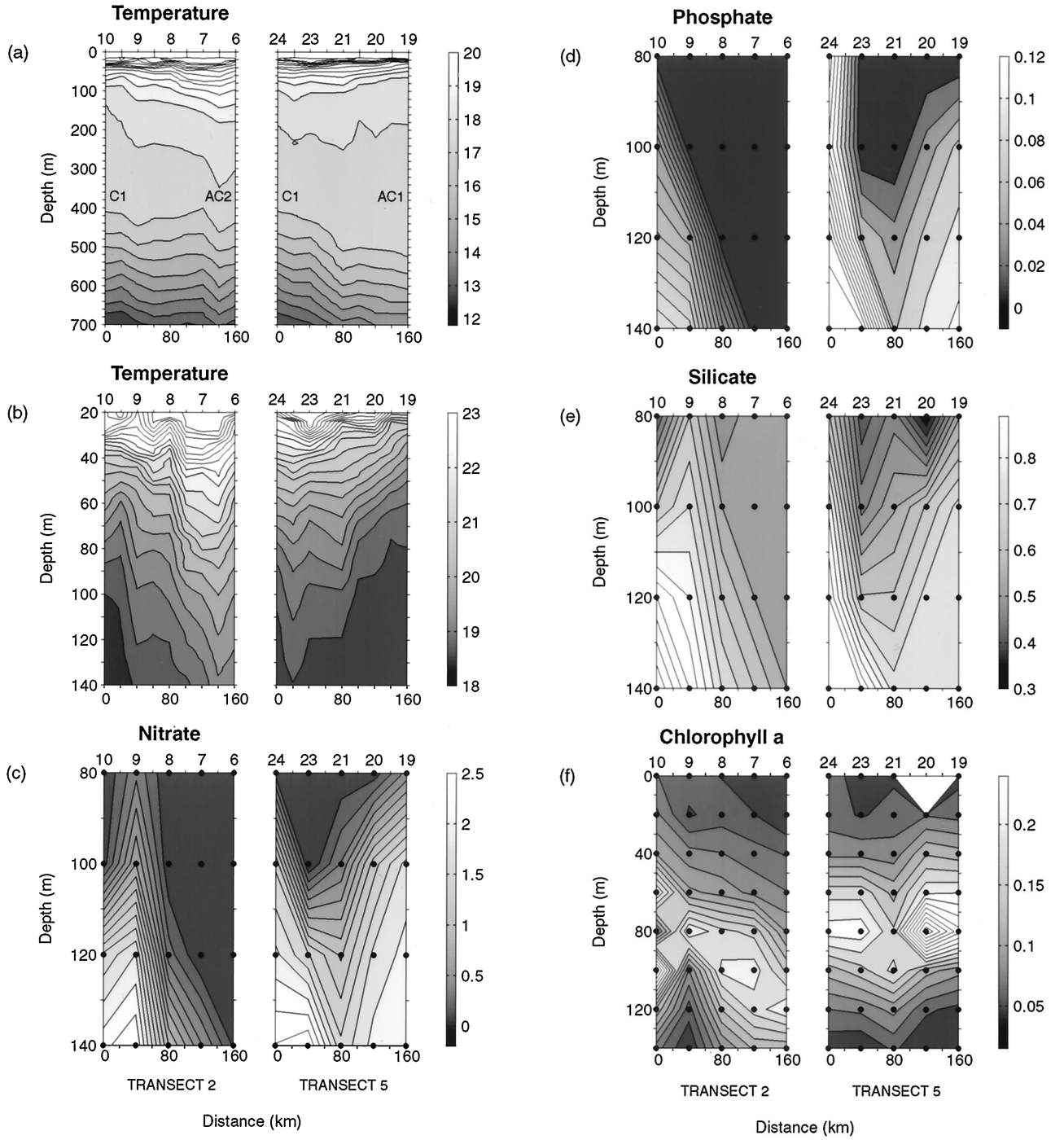

Figure 2. Vertical sections of (a) temperature (0–700 m), (b) temperature (20–140 m), (c) nitrate, (d) phosphate, (e) silicate, and (f) chlorophyll *a* on transects (left) 2 and (right) 5. Station numbers are indicated on the top of each panel. Note the difference in vertical scales for temperature (0–700 and 20–140 m), nutrient (80–140 m), and pigment (0–140 m) distributions. Units for nutrient and pigment concentrations are mmol m^{-3} and mg m^{-3}, respectively.

(Plate 2e) generally corresponds to the nitrate and phosphate distributions just below the euphotic zone. Although the correlation is not exact, chlorophyll is generally lower above the warmer, nutrient-depleted waters and higher above colder, more nutrient-rich areas. Similar patterns are present when the data are averaged over the full depth range of sampling (0–140 m) (not shown).

In interpreting the maps presented in Plate 2, care must be taken to recognize the limitations of the sampling pattern. Deployment of XBTs in between CTD stations effectively doubled the along-track resolution of the temperature field, providing satisfactory resolution of the physics. However, the spatial resolution of the CTDs is just barely sufficient to resolve the mesoscale biogeochemical variations. The major features are represented, but certainly not oversampled. Submesoscale variations are present, but not fully resolved. Finally, there are

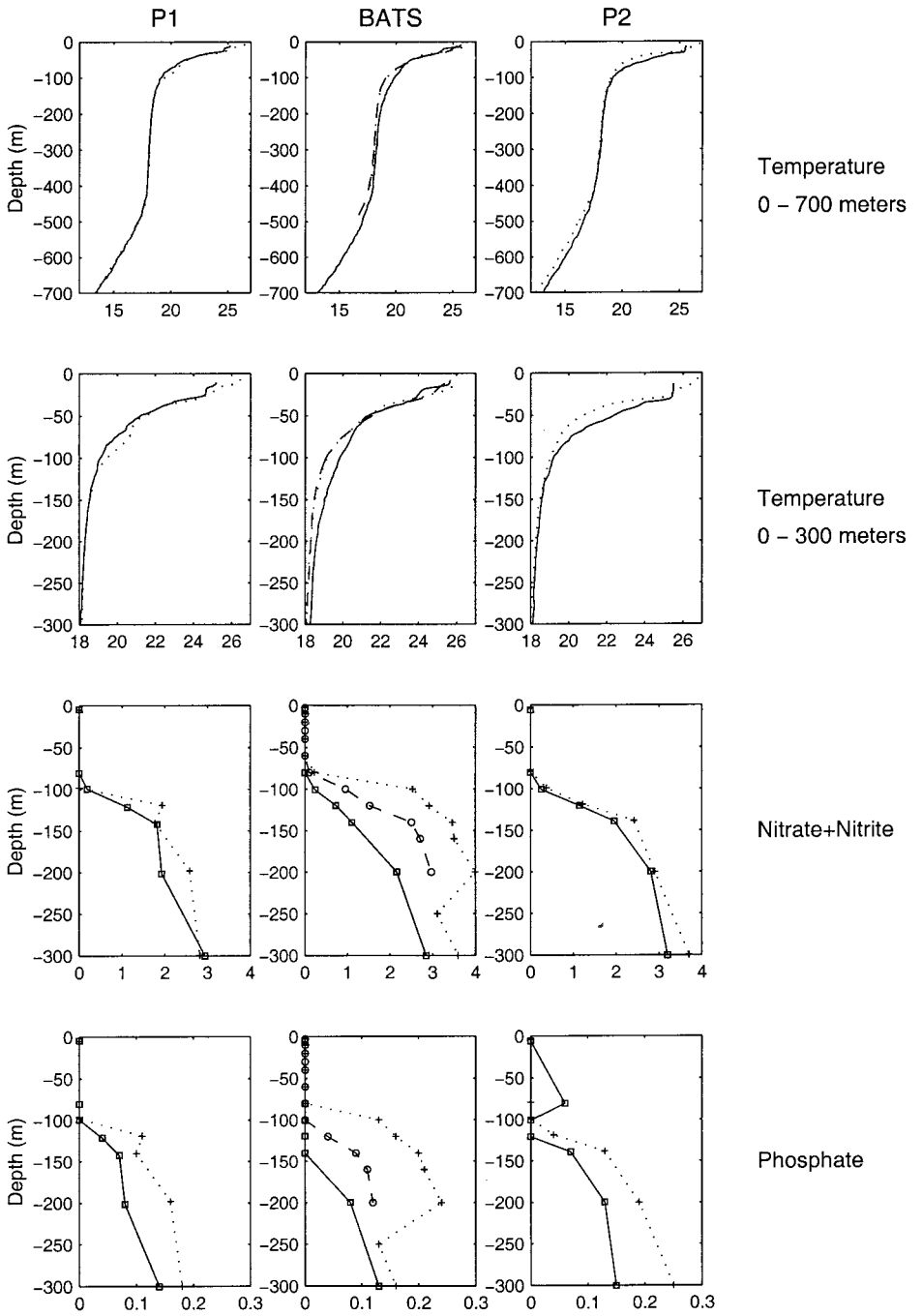

Figure 3. Temporal evolution of profiles at (left) point P1, (middle) the BATS site, and (right) point P2. Profiles from BVAL 16 (June 26–30) are indicated by solid lines with squares at data points, BBOP cruise 96.1 by dashed lines with circles, and BATS cruise 94 by dotted lines with pluses. Multiple casts taken at the BATS site during BATS cruise 94 were averaged to obtain the mean profile reported here. Units are temperature (°C), nutrients (mmol m^{-3}), and chlorophyll (mg m^{-3}).

gaps in sampling, most notably at 32.5°N, 62.8°W, where the contouring routine produces a feature of low phosphate, silicate, and chlorophyll which is clearly an artifact.

3.5. Temporal Changes

Additional observations documenting temporal evolution in biogeochemical properties are available at the three points (BATS, P1, and P2) identified in Plate 1 and Figure 1. The BATS site was revisited twice after the initial survey: on July 5 (BBOP cruise 96.1) and July 12 (BATS cruise 94). Points P1 and P2 were resampled only once, during BATS cruise 94. Sequences of profiles at the three points (Figure 3) demonstrate significant changes in physical and biogeochemical properties during the 2-week time period. The observed trends are attributable to evolution of the mesoscale physical environment documented in the model hindcast (Plate 1), although explanations based on other sources of variability are possible. During the initial survey, point P1 was flanked by the southwestern quadrant

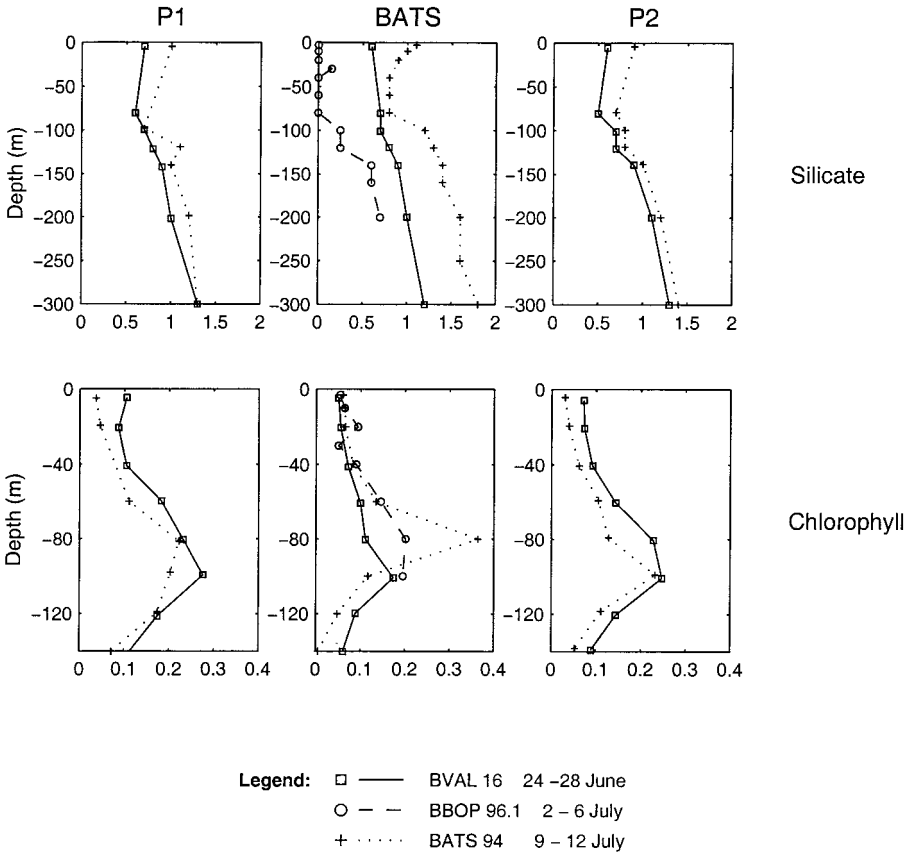

Figure 3. (continued)

of cyclone C1, while point P2 lay in the interior of cyclone C2. At that time, the BATS site was sandwiched between the two features. The merger event that takes place during the course of the following 2 weeks affects changes of varying magnitude at the three points.

Point P1 is the least affected, as the bulk of the merger activity occurs to the south and east of that location. Only minor differences in temperature structure at that location are visible 2 weeks after the initial survey (Figure 3, left). Although there is little change in the deep hydrographic structure at P1, moderate increases in nitrate, phosphate, and silicate are evident. These nutrient enhancements accompany complex temperature changes in the upper ocean: near-surface heating presumably caused by solar radiation and an increase of approximately 1°C in the 60- to 90-m depth interval. The latter is apparently driven by some sort of submesoscale variability, the nature of which is not known. Because the horizontal scale of such fluctuations is not resolved by the sampling grid, little more can be said about this issue using these data.

Moderate changes occur at point P2 as the center of cyclone C2 is drawn northeastward during its coalescence with C1. After the eddy merger is complete, P2 lies in the high-velocity region of the emergent cyclone C1/C2. Temperature profiles reveal cooling at all depths, with the exception of the upper 20 m, which is presumably warmed by surface heating (Figure 3, right). The cooling results from upward isotherm displacement associated with the formation of C1/C2. Nitrate, phosphate, and silicate increase at all depths where concentrations are detectable, commensurate with the eddy-induced upwelling. Changes in chlorophyll are qualitatively similar to those observed at P1, with a modest decrease that is fairly uniform with depth.

The most dramatic evolution in biogeochemical properties takes place at the BATS site, as the newly formed cyclone C1/C2 impinges upon that location through westward propagation. Arrival of the feature into a previously quiescent area is signaled by substantial shoaling of the main thermocline (Figure 3, middle), which causes temperatures to decrease and nutrients to increase in the upper ocean. The subsurface chlorophyll maximum shoals by 20 m and nearly doubles in magnitude. Although these aspects of the chlorophyll profile are largely controlled by one data point (the value at 80 m), the changes are consistent with those observed in high vertical resolution fluorescence data collected on the CTD (not shown). No systematic trend is evident in chlorophyll concentration above the subsurface maximum (0–60 m). A notable exception to the trend in nutrient concentration is present in the silicate profile from BBOP 96.1, which shows almost complete depletion from the surface down to 80 m. Whether or not this is symptomatic of a diatom bloom remains an open question because there are unfortunately no corresponding data on pigment composition for that station. It is important to note that analytical uncertainty is relatively large at these low levels of concentration; however, we can find no reason to suspect a systematic problem with the data in this profile.

4. Discussion

The Sargasso Sea is populated with mesoscale eddies of several different types [*Richardson*, 1993]. Typical mid-ocean eddies consist of vertical displacements of the main thermocline in either direction, with cyclones and anticyclones thus associated with cold and warm temperature anomalies, respec-

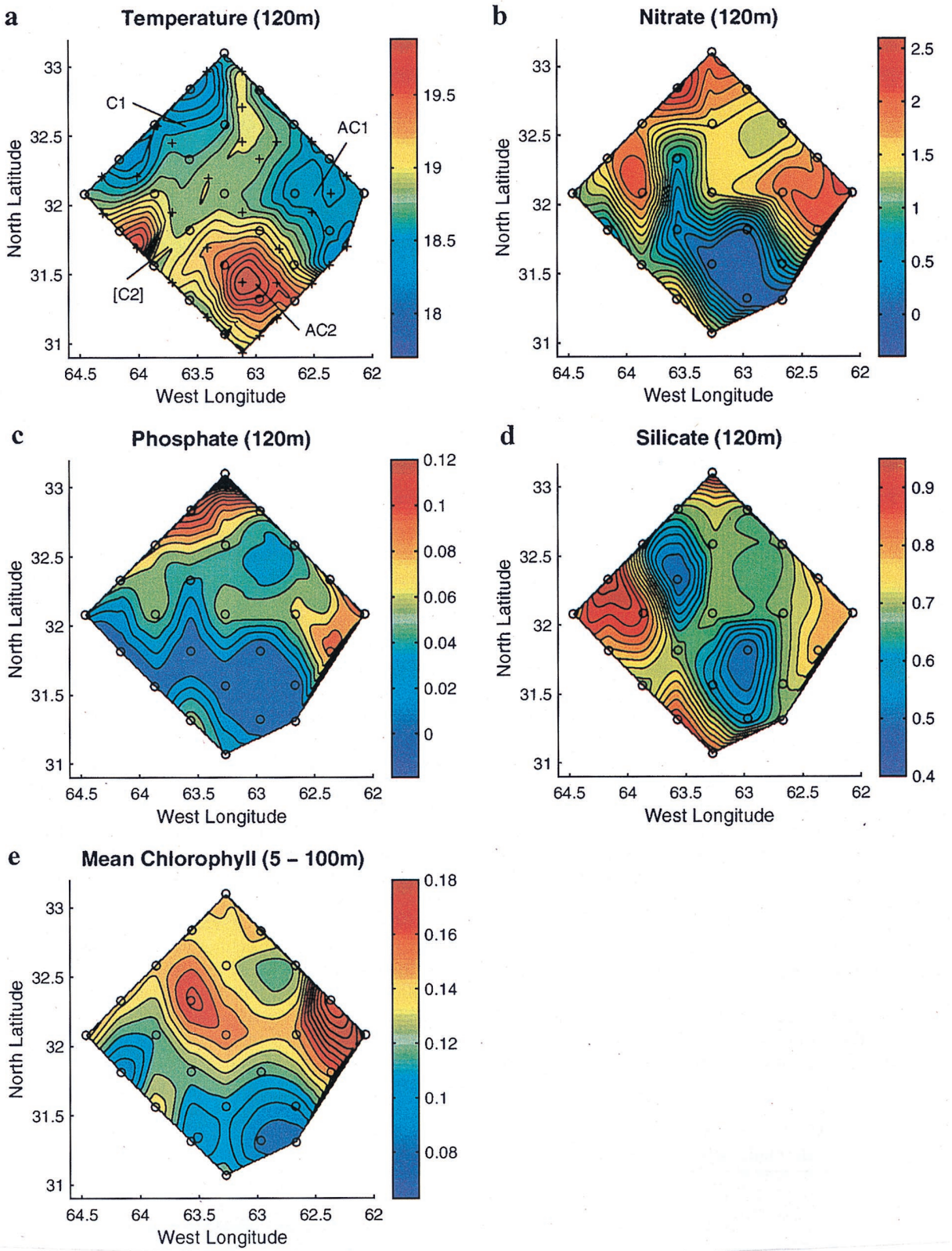

Plate 2. Results from a mesoscale biogeochemical survey near the BATS site occupied from June 24–28 1996: (a) temperature at 120 m, (b) nitrate at 120 m, (c) phosphate at 120 m, (d) silicate at 120 m, and (e) 5- to 100-m mean chlorophyll *a*. Units for nutrient and pigment concentrations are mmol m^{-3} and mg m^{-3}, respectively. Circles and crosses show locations of hydrographic stations and XBT casts, respectively. Mesoscale features identified in Plate 1 are indicated in Plate 2a; note that the near-surface expression of cyclone C2 is obscured (see text).

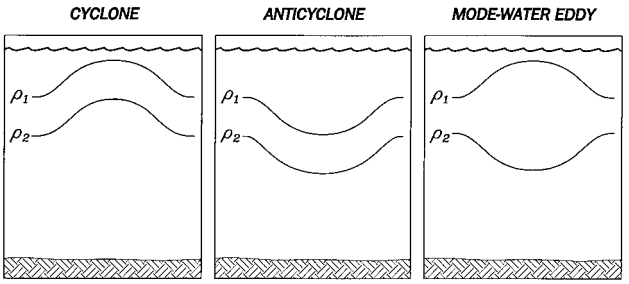

Figure 4. Isopycnal displacements associated with the various types of eddies (see text). Two density surfaces are depicted: one in the seasonal thermocline (ρ_1) and one in the main thermocline (ρ_2).

tively. This type of eddy appears to be by far the most common at the BATS site [*Siegel et al*., this issue]. The exact mechanism of their formation is not known, but they are ubiquitous features of the circulation in this region [*Richman et al*., 1977; *The MODE Group*, 1978] with water mass characteristics that indicate an origin within the Sargasso Sea. Eddies generated elsewhere frequently propagate into the Sargasso Sea, but their appearance at BATS is rare [*Siegel et al*., this issue]. Cold-core rings formed by large-amplitude meanders of the Gulf Stream transport continental slope waters across the stream into the interior of the main subtropical gyre. Larger cyclonic rings with diameters of 200 km or more have also been observed [*McCartney et al*., 1978], which are apparently formed in the Gulf Stream extension region east of 60°W. Intrathermocline lenses of several different types have also been identified in this region. *Brundage and Dugan* [1986] (hereinafter referred to as BD86) describe observations of an anticyclone consisting of a thick (500 m) bolus of 18°C water, which they hypothesize was formed by convective overturning near the New England Seamount Chain during the previous winter. This "mode water eddy" had a mesoscale horizontal dimension (170 km). A diverse phenomenology of smaller-scale features referred to as submesoscale coherent vortices has been reviewed by *McWilliams* [1985]. Lenses of water from as far away as the Gulf of Cadiz [*Zantopp and Leaman*, 1982] and the Mediterranean [*McDowell and Rossby*, 1978] have been found in the deep thermocline in the western North Atlantic.

The key issue with respect to the biogeochemical impact of eddies is the deflection of isopycnals at the base of the euphotic zone (as described in the Introduction). In terms of this particular aspect, the various sorts of eddies described above can be conveniently categorized into two types of vertical structures: (1) simple perturbations (mode 1) of the main thermocline, which extend upward toward the surface such that the displacement of the seasonal thermocline is in the same sense (the first baroclinic mode; see *Gill* [1982]), and (2) upper thermocline lenses, which tend to depress the main thermocline while lifting the seasonal thermocline (mode 2 vertical structure). A schematic view of the isopycnal displacements associated with the various types of eddies is shown in Figure 4. The first category includes eddies of both signs: cyclones that upwell nutrient-rich water into the euphotic zone and anticyclones that downwell nutrient-depleted water out of the euphotic zone. Features in the second category are generally associated with anticyclonic rotation because their displacement of the main thermocline overshadows that of the seasonal thermocline in terms of geostrophic shear. However, the sense of the isopycnal displacements in the upper ocean is the same as mode 1 cyclones.

The data set presented here documents mesoscale features with both types of vertical structure (Table 1). Cyclone C1 and anticyclone AC2 were both mode 1 features, the former enhancing nutrient concentrations at the base of the euphotic zone and the latter depleting them. The near-surface signature of weak cyclone C2 appears to have been strongly influenced by interaction with AC2, and thus its coherence in the vertical is not completely clear. On the other hand, the vertical structure of AC1 is unmistakable: the thick lens of 18°C water lifts the seasonal thermocline and depresses the main thermocline. Stations within this feature (17–21) stand out with a layer of 18°C more than 100 m thicker than the rest (Figure 5). Salinity values on the 18°C isotherm in AC1 fall within the range of other features observed in the survey, suggesting an origin within the Sargasso Sea. From a phenomenological viewpoint, AC1 is quite similar to the mode water eddy observed near 30°N, 69°W by BD86 in terms of its horizontal and vertical dimensions as well as its water mass characteristics. Although the 18°C thickness is slightly less than the 500 m observed in BD86, this could be a result of the fact that the exact center of AC1 may not have been sampled in the survey. However, the temperature and salinity structures of AC1 are very much the same as in BD86, with water mass properties consistent with the "saline mode" of 18°C water identified by *Ebbesmeyer and Lindstrom* [1986] in the POLYMODE Local Dynamics Experiment. Similar vertical structures have been observed occasionally (three times in 8 years) at BATS [*Siegel et al*., this issue] and also at the nearby *Panuliris* site [*Talley and Raymer*, 1982].

Isopycnal displacements associated with this suite of features have a discernible impact on the character of the nitrate-density relationship in the upper ocean (Figure 6). The general

Table 1. Physical Oceanographic Characteristics of Mesoscale Features Observed During the Bermuda Atlantic Time-series Study Validation Cruise BVAL16

	Feature Type		
	Cyclone	Anticyclone	Mode Water Eddy
Temperature Signal			
Near-surface	cold	warm	cold
Main thermocline	cold	warm	warm
Sea level anomaly	low	high	high
Rotation	counterclockwise	clockwise	clockwise
Features observed during BVAL16	C1, C2	AC2	AC1

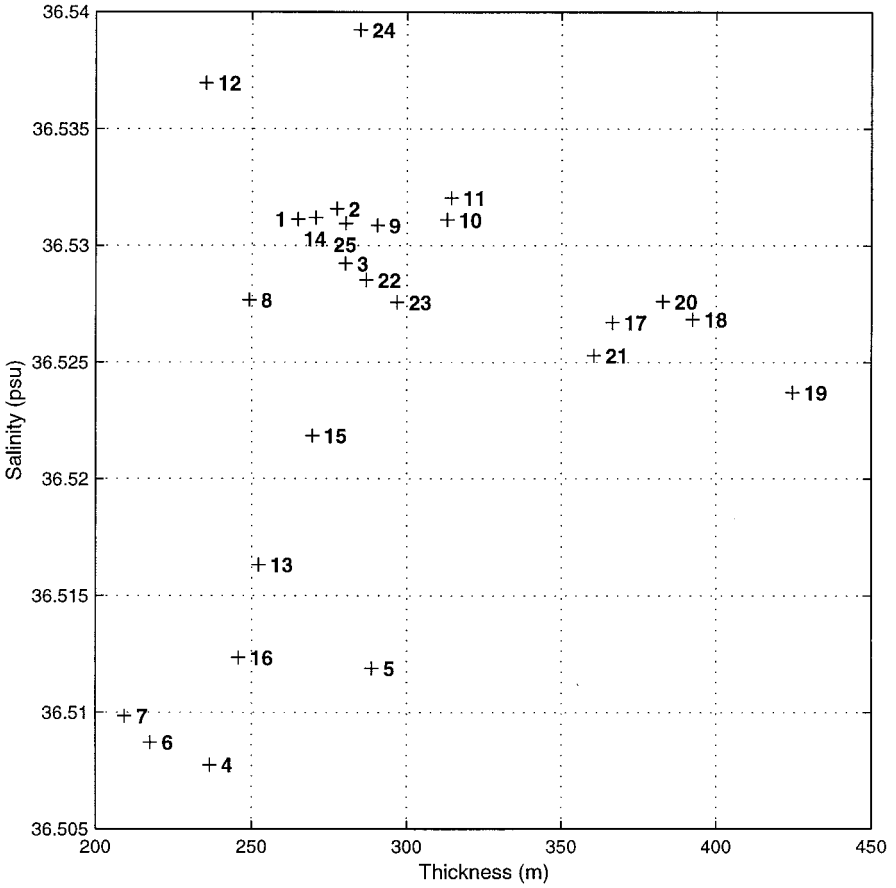

Figure 5. Salinity on the 18°C isotherm plotted versus thickness of the layer between 17.5° and 18.5°C for each of the CTD stations shown in Figure 1.

characteristics of this relationship are determined by biological uptake in the euphotic zone and remineralization of sinking particulate material below. Nutrient depletion in the well-lit surface waters results in nitrate concentrations that are independent of density, while a nearly linear relation ($r^2 = 0.89$, where r^2 is the correlation coefficient) exists at 140 m. It is at the base of the euphotic zone (100 m) where eddy-induced nutrient transport is most evident. Shoaling isopycnals in the interiors of cyclone C1 and anticyclone AC1 (circles and squares in Figure 6, respectively) cause departures from the linear relationship present in the aphotic zone. As the uplifted density surfaces within these features are illuminated, nitrate removal by the biota tends to collapse the points onto the σ_θ axis. Farther up in the euphotic zone, eddy-driven nutrient enhancement is barely detectable because the timescale for utilization (order days) is so rapid with respect to that of the supply mechanism (weeks to months). Only in the largest-amplitude isopycnal displacement (in the interior of AC1) is significant nitrate present at the 80-m depth horizon. Note that eddy-induced downwelling of nutrient-poor water from the euphotic zone is also evident in Figure 6: the depressed isopycnals of anticyclone AC2 (indicated by triangles) cause nitrate depletion all the way down to 120 m in its interior.

Similar phenomenology occurs in the BATS record. Figure 6b shows the nitrate-density relationship observed from June through August in the time series available to date. This seasonal window was chosen to exclude periods of significant mixed layer variation (and associated diapycnal transport) that occur at other times during the year. As in the BVAL16 observations, the linear relationship between nitrate and density present in the aphotic zone gradually degrades moving upward into the euphotic zone. There is clearly more scatter about this relationship in the BATS record, owing to other sources of variability such as lower-frequency interannual fluctuations. However, the changing character of this relationship with depth reveals similar phenomenology to that present in the BVAL16 data.

An idealized mechanistic sketch of this interpretation is presented in Figure 6c. In the absence of eddies, the nitrate-density relationship would occupy the dashed line in the three-dimensional representation shown in Figure 6c. Eddy fluctuations result in a distribution of density values observed at each depth horizon, the envelope of which is determined by the amplitude of the isopycnal displacements. These variations cause the character of the nitrate-density relationship to change with depth. In the aphotic zone, the corresponding range in nitrate values is well described by a linear relationship with density. In contrast, nitrate and density are not related in the upper portion of the euphotic zone; the effects of eddy upwelling are not detectable in the nutrient data because the nutrients have already been stripped out prior to the arrival of an upwelled isopycnal at that depth horizon. At the base of the euphotic zone, the situation is quite different: both eddy motions and biological uptake play a role. In the downwelling case, deepening of nutrient-depleted isopycnals is reflected in movement to the left along the σ_θ axis from the mean density

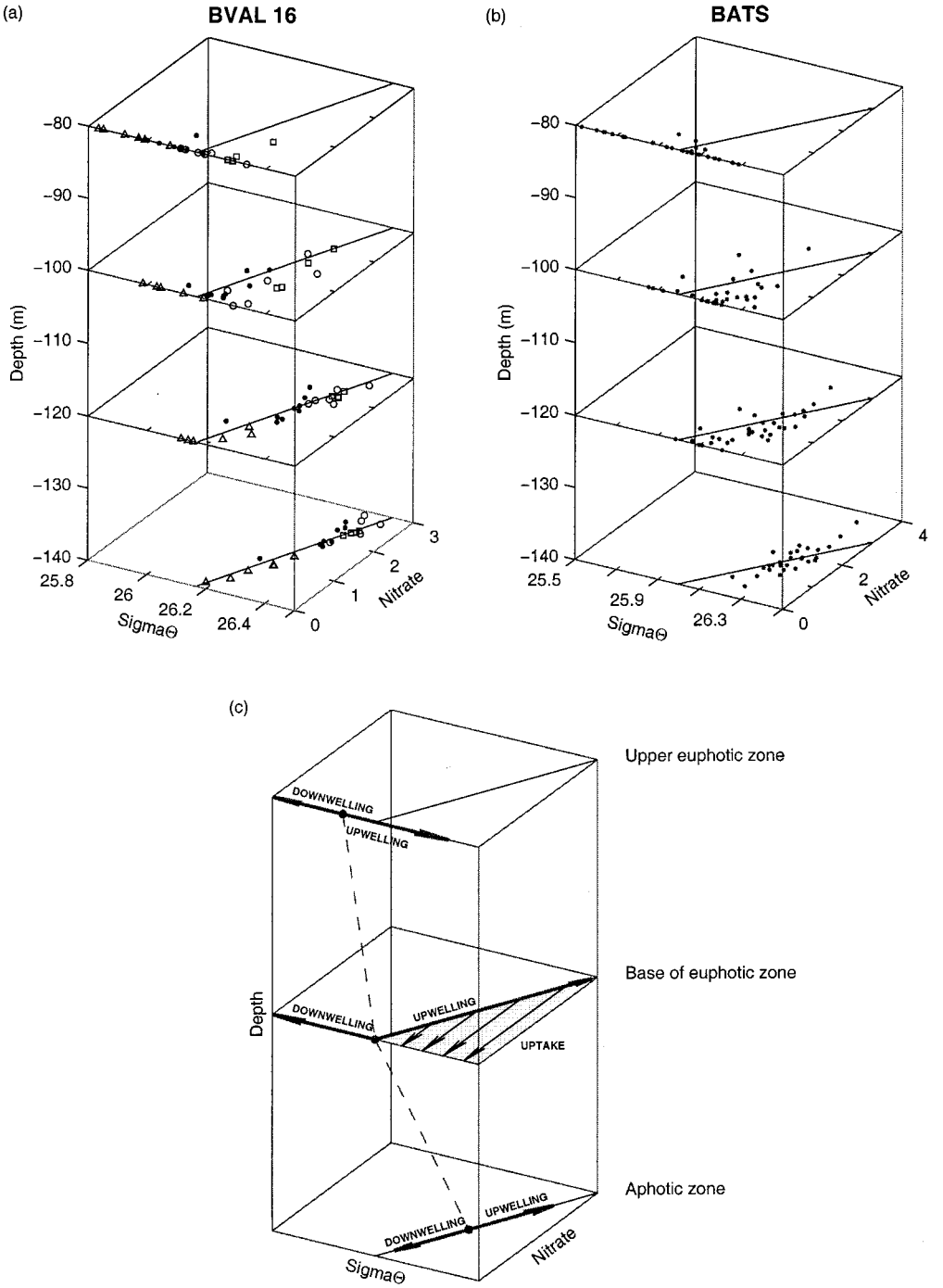

Figure 6. Nitrate (mmol m^{-3}) plotted as a function of σ_θ at various depths for (a) the BVAL16 survey and (b) summertime (June through August) BATS observations from 1989 to 1996. In Figure 6a, different symbols indicate stations falling within the three strongest mesoscale features. Circles, squares, and triangles represent C1, AC1, and AC2, respectively. Dots show stations in between these features. (c) Cartoon sketch providing a mechanistic interpretation of these data (see text). The dashed line represents what the nitrate-density relationship would look like in the absence of vertical isopycnal displacements associated with eddies.

at that depth where the nitrate concentration is zero. Upwelling tends to introduce nutrient-rich waters into the illuminated surface layers; this amounts to moving upward along the linear increase in nitrate. Subsequent uptake by phytoplankton pulls the nitrate concentrations down, causing departures from the linear relation. In a mature eddy where upwelling has ceased and the biological response is complete, nutrients will be entirely depleted. Up until that time, nitrate values will fall somewhere in between the linear relationship maintained below and zero (the shaded area in Figure 6c). Thus eddy-induced upwelling essentially deepens the nitracline by intermittently exposing waters from below to light.

Finally, it is of interest to consider the magnitude of the variability observed during BVAL16 with that from the BATS

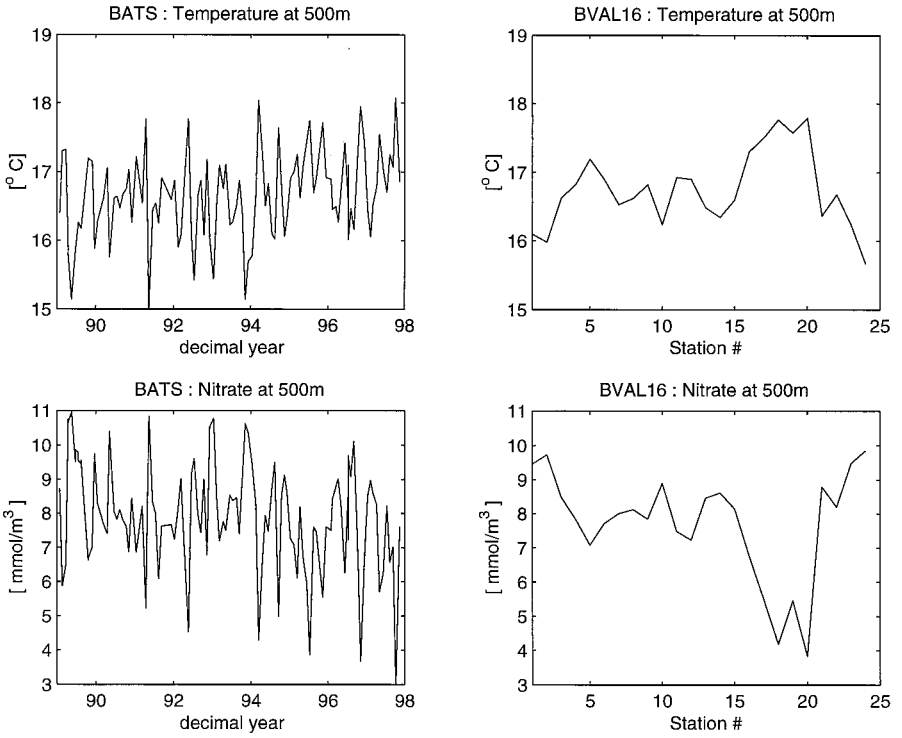

Figure 7. Temperature (°C) and nitrate (mmol m^{-3}) at 500 m observed in the 1988–1998 (left) BATS time series and (right) BVAL16 spatial survey.

time series record. Analysis of the BATS physical and nutrient data at fixed depths within the main thermocline reveals significant variability on the timescale of the monthly sampling frequency (Figure 7). The variability observed at the same depth horizons during the BVAL16 spatial survey was statistically similar to the 10-year BATS time series (Table 2). For example, nitrate concentrations at 500 m at BATS range from 3–11 mmol m^{-3} with a mean of 7.9 ± 1.6 mmol m^{-3}, while for BVAL 16, the corresponding values are 4–10 mmol m^{-3} and 7.7 ± 1.6 mmol m^{-3}. Thermocline variability at BATS appears to be strongly driven by isopycnal displacements of similar magnitude to that observed within cyclonic and anticyclonic eddies. It seems reasonable to conclude that passage of these features through the time series site dominates the temporal variance of the thermocline observed at BATS on monthly timescales. Of course, the situation is not so clear-cut in the upper ocean, where surface forcing and thermocline-driven processes interact. Detailed diagnosis of the their relative contributions to variability in the BATS record of upper ocean biogeochemical properties is the subject of future work.

Table 2. Comparison of Statistics From 1988–1998 BATS Time Series and BVAL16 Survey for Temperature and Nitrate at 500 m

	BATS, 1989–1998		BVAL16	
	Temperature, °C	Nitrate, mmol m^{-3}	Temperature, °C	Nitrate, mmol m^{-3}
Mean	16.64	7.92	16.75	7.71
Standard deviation	0.64	1.62	0.56	1.60
Minimum	14.99	2.95	15.67	3.84
Maximum	18.08	10.96	17.79	9.85

5. Summary and Conclusions

The long history of time series measurements near Bermuda has documented a wealth of transient variations that have been attributed to the passage of mesoscale features [*Jenkins*, 1988; *Malone et al*., 1993; *Roman et al*., 1993; *Siegel et al*., 1995; *Doney*, 1996; *McGillicuddy et al*., 1998; *McNeil et al*., 1999]. However, in most cases the lack of spatial information inherent in fixed-point time series records has precluded definitive differentiation between spatial and temporal variability. Here we have presented a coupled modeling and observational strategy capable of explicitly resolving the four-dimensional nature of the processes by which mesoscale ocean dynamics influences upper ocean biogeochemistry. Real-time nowcasting and forecasting of the flow field during biogeochemical survey operations facilitated strategic sampling of several eddy features. Large spatial variations in nutrient availability (from undetectable to in excess of 2 mmol NO_3 m^{-3}) at the base of the euphotic zone resulted from vertical isopycnal displacements associated with the eddies. Although somewhat noisier, phytoplankton biomass patterns generally corresponded to nutrient distributions. Increased phytoplankton biomass in the waters overlying nutrient enhancements implied eddy-induced nutrient transport from below. The nutrient injections were brought about by two different types of eddies: a typical mid-ocean cyclone that domed both the main and seasonal thermoclines upward and a mode water eddy consisting of a thick lens of 18°C water that lifted the seasonal thermocline while depressing the main thermocline. Hindcast simulations carried out for the 2 weeks follow-

ing the survey provide a four-dimensional context in which to interpret additional time series observations at and near BATS site. During that time, two cyclones present during the initial survey merged to form a new cyclone that propagated west and impinged upon the BATS site. Temporal trends in physical and biogeochemical properties observed at BATS were generally consistent with the arrival of a mid-ocean cyclone: domed isopycnals, increased nutrient availability at the base of the euphotic zone, and higher phytoplankton biomass within the euphotic zone.

Acknowledgments. We gratefully acknowledge the support of JPL, NASA, and NSF. Special thanks to Olga Kosnyreva and Peter Hlavaty, who contributed a great deal to the processing and analysis of the data, and also to Betsey Doherty, who drafted Figure 4. The exceptional efforts of the BATS technicians are greatly appreciated. The comments of two anonymous reviewers helped improve the manuscript. This is WHOI contribution 9792.

References

Bates, N. R., A. F. Micheals, and A. H. Knap, Spatial variability of CO_2 species in the Sargasso Sea, *Caribbean J. Sci*., *32*, 262, 1996.

Brundage, W. L., and J. P. Dugan, Observations of an anticyclonic eddy of 18° water in the Sargasso Sea, *J. Phys. Oceanogr*., *16*, 717–727, 1986.

Carter, E. F., and A. R. Robinson, Analysis models for the estimation of oceanic fields, *J. Atmos. Oceanic Technol*., *4*(1), 49–74, 1987.

Carton, J. A., How predictable are the geostrophic currents in the recirculation zone of the North Atlantic?, *J. Phys. Oceanogr*., *17*, 751–762, 1987.

Carton, J. A., and D. J. McGillicuddy, Comprehensive maps of POLYMODE streamfunction, *Rep. Meteor. Oceanogr*., *21*, Div. of Appl. Sci., Harvard Univ., Cambridge, Mass., 1985.

Doney, S. C., A synoptic atmospheric surface forcing data set and physical upper ocean model for the U.S. JGOFS Bermuda Atlantic Time Series (BATS) site, *J. Geophys. Res*., *101*, 25,615–25,634, 1996.

Ebbesmeyer, C. C., and E. J. Lindstrom, Structure and origin of 18°C water observed during the POLYMODE Local Dynamics Experiment, *J. Phys. Oceanogr*., *16*, 443–453, 1986.

Eppley, R. W., Temperature and phytoplankton growth in the sea, *Fish. Bull*., *17*, 15–24, 1972.

Gill, A. E., *Atmosphere-Ocean Dynamics*, Academic, San Diego, Calif., 1982.

Harrison, D. E., and R. H. Heinmiller, Upper ocean variability in the Sargasso Sea July 1977–July 1978: The POLYMODE XBT program, *J. Phys. Oceanogr*., *13*, 859–872, 1983.

Jenkins, W. J., The use of anthropogenic tritium and helium-3 to study subtropical gyre ventilation and circulation, *Philos. Trans. R. Soc*., *London Ser. A*, *325*, 43–61, 1988.

Knap, A. H., et al., BATS methods manual, technical report, U.S. JGOFS Plann. Off., Woods Hole, Mass., 1993.

Malone, T. C., S. E. Pike, and D. J. Conley, Transient variations in phytoplankton productivity at the JGOFS Bermuda time series station, *Deep Sea Res*., *Part I*, *40*, 903–924, 1993.

McCartney, M. S., L. V. Worthington, and W. J. Schmitz, Large cyclonic rings from the northeast Sargasso Sea, *J. Geophys. Res*., *83*, 901–914, 1978.

McDowell, S. E., and H. T. Rossby, Mediterranean water: An intense mesoscale eddy off the Bahamas, *Science*, *202*, 1085–1087, 1978.

McGillicuddy, D. J., and A. R. Robinson, Eddy induced nutrient supply and new production in the Sargasso Sea, *Deep Sea Res*., *Part I*, *44*, 1427–1449, 1997.

McGillicuddy, D. J., A. R. Robinson, D. A. Siegel, H. W. Jannasch, R. Johnson, T. D. Dickey, J. McNeil, A. F. Michaels, and A. H. Knap, Influence of mesoscale eddies on new production in the Sargasso Sea, *Nature*, *394*, 263–265, 1998.

McNeil, J. D., H. W. Jannasch, T. Dickey, D. McGillicuddy, M. Brzezinski, and C. M. Sakamoto, New chemical, bio-optical, and physical observations of upper ocean response to the passage of a mesoscale eddy off Bermuda, *J. Geophys. Res.*, in press, 1999.

McWilliams, J. C., Submesoscale, coherent vortices in the ocean, *Rev. Geophys*., *23*, 165–182, 1985.

Michaels, A. F., Ocean time series research near Bermuda: The Hydrostation S time series and the Bermuda Atlantic Time-series Study program, in *Ecological Time Series*, edited by T. Powell and J. Steele, pp. 181–208, Chapman and Hall, New York, 1995.

Michaels, A. F., and A. H. Knap, An overview of the U.S. JGOFS Bermuda Atlantic Time-series study and the Hydrostation S program, *Deep Sea Res*., *Part II*, *43*, 157–198, 1996.

Michaels, A. F., et al., Seasonal patterns of ocean biogeochemistry at the U.S. JGOFS Bermuda Atlantic Time-series Study site, *Deep Sea Res*., *Part I*, *41*, 1013–1038, 1994.

Richardson, P. L., A census of eddies observed in North Atlantic SOFAR float data, *Prog. Oceanogr*., *31*, 1–50, 1993.

Richman, J. G., C. Wunsch, and N. G. Hogg, Space and time scales of mesoscale motion in the western North Atlantic, *Rev. Geophys*., *15*, 385–420, 1977.

Robinson, A. R., and W. G. Leslie, Estimation and prediction of oceanic eddy fields, *Prog. Oceanogr*., *14*, 485–510, 1985.

Robinson, A. R., and L. J. Walstad, The Harvard Open Ocean Model: Calibration and application to dynamical process, forecasting, and data assimilation studies, *Appl. Numer. Math*., *3*(1–2), 89–131, 1987.

Roman, M. R., H. G. Dam, A. L. Gauzens, and J. M. Napp, Zooplankton biomass and grazing at the JGOFS Sargasso Sea time series station, *Deep Sea Res*., *Part I*, *40*, 883–901, 1993.

Siegel, D. A., A. F. Michaels, J. C. Sorenson, M. C. O'Brien, and M. A. Hammer, Seasonal variability of light availability and utilization in the Sargasso Sea, *J. Geophys. Res*., *100*, 8695–8713, 1995.

Siegel, D. A., D. J. McGillicuddy, Jr., and E. A. Fields, Mesoscale eddies, satellite altimetry, and new production in the Sargasso Sea, *J. Geophys. Res*., this issue.

Talley, L. D., and M. E. Raymer, Eighteen degree water variability, *J. Mar. Res*., *40*, 757–775, 1982.

The MODE Group, The Mid-Ocean Dynamics Experiment, *Deep Sea Res*., *25*, 859–910, 1978.

Walstad, L. J., and A. R. Robinson, Hindcasting and forecasting of the POLYMODE data set with the Harvard open ocean model, *J. Phys. Oceanogr*., *20*, 1682–1702, 1990.

Zantopp, R., and K. Leaman, Gulf of Cadiz water observed in a thermocline eddy in the western North Atlantic, *J. Geophys. Res*., *87*, 1927–1934, 1982.

N. R. Bates, R. Johnson, and A. H. Knap, Bermuda Biological Station for Research, Ferry Reach, GE01, Bermuda.

D. J. McGillicuddy Jr. (corresponding author), Department of Applied Ocean Physics and Engineering, Woods Hole Oceanographic Institution, Woods Hole, MA 02543. (dmcgillicuddy@whoi.edu)

A. F. Michaels, Wrigley Institute for Environmental Studies, University of Southern California, Avalon, CA 90704.

D. A. Siegel, Institute for Computational Earth System Science, University of California, Santa Barbara, CA 93106.

(Received September 9, 1998; revised January 20, 1999;
accepted January 29, 1999.)